CORE
Metadata, citation and similar papers at core.ac.uk
Provided by UNL | Libraries

University of Nebraska - Lincoln
DigitalCommons@University of Nebraska - Lincoln

Stephen Ducharme Publications | Research Papers in Physics and Astronomy

5-2014

Polarization imaging in ferroelectric polymer thin film capacitors by pyroelectric scanning microscopy

Jingfeng Song
University of Nebraska-Lincoln, jsong4@unl.edu

Haidong Lu
University of Nebraska-Lincoln, s-hlu4@unl.edu

Alexei Gruverman
University of Nebraska-Lincoln, agruverman2@unl.edu

Stephen Ducharme
University of Nebraska-Lincoln, sducharme1@unl.edu

Follow this and additional works at: http://digitalcommons.unl.edu/physicsducharme

Part of the Condensed Matter Physics Commons

Song, Jingfeng; Lu, Haidong; Gruverman, Alexei; and Ducharme, Stephen, "Polarization imaging in ferroelectric polymer thin film capacitors by pyroelectric scanning microscopy" (2014). *Stephen Ducharme Publications*. 96.
http://digitalcommons.unl.edu/physicsducharme/96

This Article is brought to you for free and open access by the Research Papers in Physics and Astronomy at DigitalCommons@University of Nebraska - Lincoln. It has been accepted for inclusion in Stephen Ducharme Publications by an authorized administrator of DigitalCommons@University of Nebraska - Lincoln.

Polarization imaging in ferroelectric polymer thin film capacitors by pyroelectric scanning microscopy

Jingfeng Song,[a] Haidong Lu, Alexei Gruverman, and S. Ducharme[b]
Department of Physics and Astronomy Nebraska Center for Materials and Nanoscience University of Nebraska, Lincoln, Nebraska 68588-0299, USA

(Received 7 April 2014; accepted 29 April 2014; published online 12 May 2014)

A Pyroelectric Scanning Microscopy system, which uses laser-induced thermal modulation for mapping the pyroelectric response, has been used to image a bipolar domain pattern in a ferroelectric polymer thin film capacitor. This system has achieved a resolution of 660 ± 28 nm by using a violet laser and high *f*-number microscope objective to reduce the optical spot size, and by operating at high modulation frequencies to reduce the thermal diffusion length. The results agree well with a thermal model implemented numerically using finite element analysis. © *2014 AIP Publishing LLC*. [http://dx.doi.org/10.1063/1.4875960]

Ferroelectric materials have been the subject of increasing interest in recent decades, largely because of the development of methods for thin film and nanostructure fabrication, and subsequent integration into a wide range of electronic technologies, such as thermometry and thermal imaging,[1,2] electromechanical transducers,[3] nonvolatile memories,[4] organic electronics,[5] and energy storage,[6] as well as promising applications to organic photovoltaics,[7] solid-state energy harvesting, and refrigeration.[8,9] To further improve the performance and utility of ferroelectric materials, it is essential to be able to measure the spatial distribution of the polarization at high resolution. The current method of choice for polarization imaging is Piezoresponse Force Microscopy (PFM),[10,11] because the piezoresponse is proportional to the net polarization. The pyroelectric response is also proportional to net polarization, but, because it is based on a different physical principle, it affords a complementary probe for imaging polarization.[12]

The Pyroelectric Scanning Microscopy (PSM) records the two-dimensional distribution of pyroelectric response by scanning a focused and modulated laser beam across a pyroelectric sample and recording the induced surface charge.[13,14] PSM works with crystals[13–19] and with thin films.[20–23] PSM has also been used to image domains[14,24] thermally written polarization patterns,[25–28] and to follow polarization and domain dynamics.[29–32] Moreover, 3D polarization information can be obtained from crystals and thick films by combining 2D laser scanning with depth profiles obtained using either pulse time-of-flight methods,[33] or Laser Intensity Modulation Method (LIMM),[34–38] or both.[39] One key advantage of PSM over techniques based on atomic force microscopy (AFM) is that the optical probe is noninvasive and does not damage or alter the sample.[40] The PSM technique, however, can only determine the component of the polarization perpendicular to the electrodes, whereas vector PFM can obtain both in-plane and out-of-plane components.[41] In addition, PFM affords higher spatial resolution, down to 10 nm,[42] whereas prior PSM studies have only achieved a spatial resolution of 2 μm.[14,39] Optimizing the resolution of PFM requires careful attention to both optical and thermal limitations in conjunction with a 3D thermal model.[34–36,43]

With these considerations in mind, we have designed a PSM system with much improved resolution by using a violet laser and high *f*-number microscope objective to reduce the optical spot size, and by operating at high modulation frequencies to reduce the thermal diffusion length. The results of these imaging studies agree well with the predictions of a thermal model implemented using finite element analysis (FEA).

The sample for the present study was prepared as follows. A 20-nm thick, 50-μm wide bottom electrode of aluminum was prepared by photolithography on a glass substrate. The copolymer of vinylidene fluoride (70%) and trifluoroethylene (30%), P(VDF-TrFE), was dissolved in dimethylsulfoxide to a concentration of 0.05% by weight. The thin film of 20 nominal monolayers, approximately 36 nm in thickness,[44] was prepared by horizontal Langmuir-Blodgett (LB) deposition at a surface pressure of 5 mN/m. The sample was annealed for 60 min at 135 °C in an air oven with heating and cooling rates of 1 °C/min. The method of sample preparation and the properties of the film thus produced are described in greater detail elsewhere.[30,45,46]

The PSM system works by scanning a tightly focused modulated laser beam across a pyroelectric capacitor and recording the modulated current from the electrodes. The apparatus shown in Fig. 2(a) consists of a computer-controlled nanopositioning system (Thorlabs NanoMax 300) using step sizes of 100 nm in 1D scans and 250 nm in 2D images. A 15 mW diode laser with wavelength $\lambda = 405$ nm was focused through a ×60 microscope objective with numerical aperture (NA) of 0.85 onto the sample. With this arrangement, the theoretical diffraction-limited focal spot diameter is $2\lambda/(\pi \mathrm{NA}) = 304$ nm.[47] The actual spot size of 352 ± 14 nm was measured using a scanning edge method. The laser power was sinusoidally modulated by a function generator (Hewlett-Packard HP 8111 A). The pyroelectric signal generated at each beam position was recorded by a lock-in amplifier (Stanford Research Systems SRS 844) with 1 MΩ input impedance and arranged into either a 1D line or a 2D array, or image, of the pyroelectric response. Topographical and polarization imaging of the ferroelectric film were done with

[a]Email: jingfsong@huskers.unl.com
[b]Email: sducharme1@unl.edu

 © 2014 AIP Publishing LLC

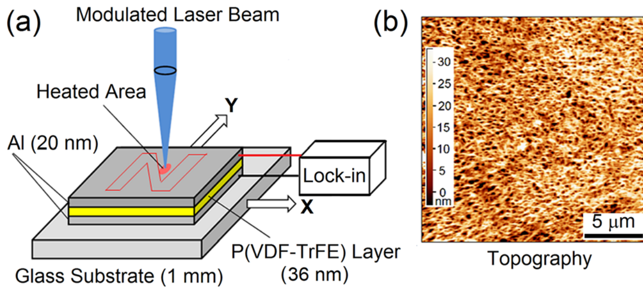

FIG. 1. (a) PSM apparatus showing the arrangement of the modulated laser beam and ferroelectric capacitor, which was translated in two dimensions by the nanopositioner (not shown). (b) Topographic image of the P(VDF-TrFE) film recorded with the AFM.

a commercial atomic force microscope (AFM, model MFP-3D from Asylum Research) using platinum-coated cantilevers (CSC17/Pt, Mikromasch) in a resonant-enhanced mode at a frequency of 170 kHz and 0.8 V modulation amplitude.

Figure 1(b) shows AFM topographic image of a 20 μm $\times$ 20 μm testing area of the P(VDF-TrFE) film. A bipolar polarization pattern was prepared on the sample using an AFM tip-poling method at a scanning rate of 1 Hz by first poling the 20 μm $\times$ 20 μm square with a +12 V tip bias, and then an "N" pattern with −12 V tip bias.[48] This produced a stable bipolar "N" pattern that is clearly evident in the PFM amplitude and phase images shown in Figs. 2(a) and 2(b). The polarization of the dark "N" patterned area points out of the film, whereas light surrounding area points into the film. The bipolar polarization "N" pattern are evident in the PFM phase image, Fig. 2(b), and have both high contrast and a high resolution of order 10 nm, as we have found before with polarization patterns prepared in similar ferroelectric copolymer LB films.[48–51]

The ferroelectric polymer film was then covered with a 20-nm thick, 200-μm wide, aluminum top electrode by thermal evaporation and then installed in the PSM apparatus for imaging [see Fig. 1(a)]. The PSM amplitude and phase images recorded at a modulation frequency $f = 1.8$ MHz shown in Figs. 2(c) and 2(d) clearly reveal the bipolar "N" pattern. The amplitude image shows a strong (red) signal everywhere except at the boundaries (in blue) between up and down polarization. Moreover, the PSM phase image in Fig. 2(d) shows a clear reversal of the normal component of the polarization in the regions poled with positive (blue) and negative (orange) voltage, which is consistent with the PFM phase image in Fig 2(b). The PSM imaging was repeated at intervals for 7 weeks, revealing no significant decay of polarization. Summarizing the PFM and PSM imaging results, we can see that the PSM system is an efficient tool in mapping the pyroelectric current distribution and polarization imaging in the ferroelectric thin film capacitors with high resolution.

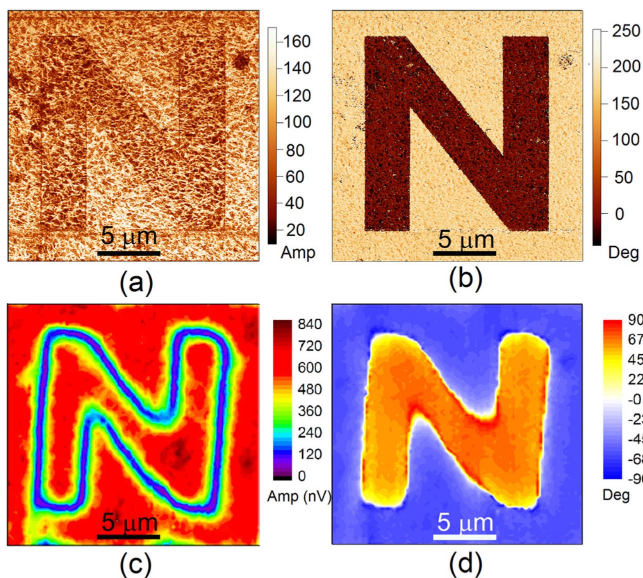

FIG. 2. Image of the "N" pattern written with the AFM Tip. The top images from the PFM measurements show the distribution of the amplitude (a) and phase (b) of the piezoresponse. The bottom images from the PSM, which were recorded 1.8 MHz laser modulation frequency, show the distribution of the amplitude (c) and phase (d) of the pyroelectric response.

Because of the limitations of optical resolution and thermal diffusion, the PSM images of amplitude and phase [Figs. 2(c) and 2(d)] have lower resolution than the corresponding PFM images [Figs. 2(a) and 2(b)]. To model the PSM images while neglecting thermal diffusion, we began by calculating the convolution of the much sharper reference PFM image with a Gaussian distribution of the local heating rate corresponding to the profile of the laser beam intensity at the sample surface. The pyroelectric current distribution J(x,y) is the convolution of the polarization pattern $P(x,y)$ from with the heating rate $g(x,y)$ as follows:[47,52]

$$J(x,y) = p \int_{-\infty}^{+\infty} P(\tau_1,\tau_2) g(x-\tau_1, y-\tau_2) d\tau_1 d\tau_2, \quad (1)$$

where p is the pyroelectric coefficient, which is approximately $-20\,\mu\text{C/m}^2\text{K}$ for the ferroelectric polymer LB films.[12] To perform the convolution, we first calculated the polarization distribution $P(x,y) = \text{Amplitude} \times \cos(\text{phase})$ shown in Fig. 3(a) from the PFM amplitude and phase data shown in Figs. 2(a) and 2(b). We then calculated the convolution according to Eq. (1) of the polarization pattern P(x,y) with a Gaussian heating rate profile $g(x,y) = g_0 \exp(-2\rho^2/s^2)$, where $\rho = x^2 + y^2$ is the lateral distance from the laser beam center. We were able to obtain excellent correspondence between the model PSM image shown in Fig. 3(b) and the actual PSM image shown in Fig. 3(c) by setting the Gaussian diameter $2s = 660$ nm. Since this is approximately twice the diameter of the laser beam waist, it appears that thermal diffusion is indeed causing additional blurring of the PSM image, even at 1.8 MHz modulation frequency.

Two observations can be made from close examination of the images in Figs 3(b) and 3(c). First, the two images exhibit the same degree of rounding and blurring at the sharp edges of the "N" pattern. Second, on close examination of the shoulder of the "N" indicated by the circles in Figs. 3(a) and 3(c), we can see that PSM not only reproduces the general character of the blurring but also details like the relatively large signal measured in the interior of the shoulder, which is furthest from the edges. A quantitative comparison was performed by taking line scans from the three images, Figs. 3(a)–3(c) to yield profiles like those shown in Fig. 3(d), showing good qualitative agreement between the actual PSM line profile and the line profile obtained from the convolution

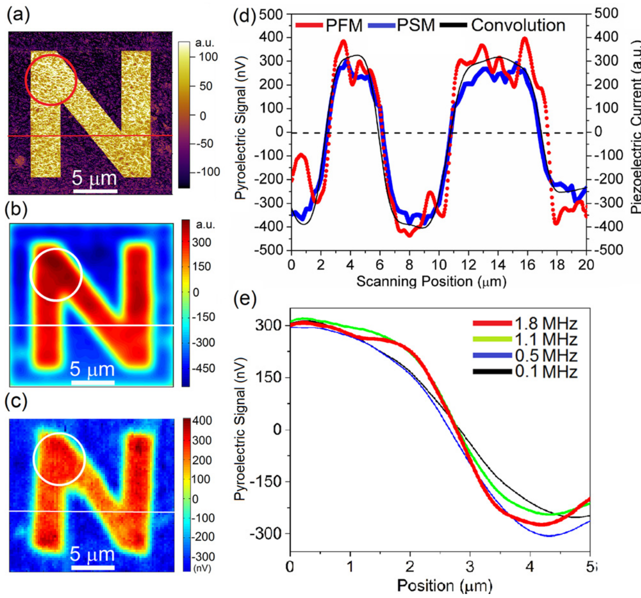

FIG. 3. Composite signal images of the form Amplitude × cos(phase) combining amplitude and phase contributions. (a) The polarization signal obtained from the PFM data shown in Figs. 2(a) and 2(b). (b) The model PSM signal calculated from the numerical convolution of the PFM signal with an effective Gaussian diameter of $2s = 660$ nm, and (c) from the PSM data shown in Figs. 2(c) and 2(d). (d) Line scans from the stripes indicated in (a)–(c). (e) Line scans across the trailing edge of the lower leg of the "N" from PSM images like the one in (c) at modulation frequencies of 0.1 MHz, 0.5 MHz, 1 MHz, and 1.8 MHz.

of the PSM image with the Gaussian beam profile. The PSM line profile reproduces calculated convolution very well.

The temperature distribution produced by a laser source having a Gaussian intensity distribution with beam diameter $2s = 304$ nm and sinusoidal temporal modulation with frequency $\omega = 2\pi f$ will have the form $T(\rho, z, t)$ in cylindrical coordinates. Assuming that the heat is entirely absorbed at the top surface of the sample, the heat flux at $z = 0$ has the form

$$\Phi(\rho, z = 0, t) = \Phi_0 e^{-\frac{2\rho^2}{s^2}}(1 - \cos\omega t). \tag{2}$$

Since the PSM images were obtained only from the modulated component of the output current, we will solve for the complex amplitude of modulated part of the temperature profile $\Delta T(\rho, z)\exp(i\omega t)$.

The sample is represented by a four-layer physical model, as shown in Fig. 4(a), consisting of 20-nm thick aluminum electrodes, a 40 nm ferroelectric copolymer film, and a thick glass substrate. The following assumptions were made in the physical model. The boundary conditions consisted of the imposed heat flux (Eq. (2)) at the top surface, continuous heat flux across the layers (Neumann condition), and a reservoir temperature of 300 K at the edges of the model volume (Dirichlet condition), a depth $z = 5\,\mu$m and radius $\rho = 10\,\mu$m from the beam axis. These distances are much larger than the thermal diffusion length and therefore constitute a sufficiently large model. The thermal impedance of the interfaces was neglected, and the thermal diffusivities and specific heat capacities respectively, of the layers were as follows:[21,53] aluminum 3.86×10^{-5} m^2/s and specific heat 900 J/Kg^{-1}K^{-1}; glass 5.97×10^{-7} m^2/s and 670 J/Kg^{-1}K^{-1}; and copolymer 5.6×10^{-8} m^2/s and 1233 J/Kg^{-1}K^{-1}.

To calculate the temperature distribution $T(\rho, z, t)$ as a function of time, and to better determine the effect of thermal diffusion on the PSM image resolution, we turned to FEA software using a commercial program (ABAQUS 6.11) on the physical model shown in Fig. 4(a).[36] The calculations were made on a 5 nm to 50 nm size mesh, at four modulation frequencies from 0.1 MHz to 1.8 MHz, using the assumptions described above. The results were not sensitive to the mesh size. The FEA model was run until the amplitude $\Delta T(\rho, z)$ of the modulated part of the temperature reached steady state, as shown in Fig. 4(b). The modulated part of the radial temperature profile $\Delta T(\rho)$ in the ferroelectric film, which was calculated by averaging the distribution $\Delta T(\rho, z)$ over the depth z, is shown in Fig. 4(c) as a function of frequency. In this way, both the laser intensity profile and thermal diffusion are accounted for in calculating the PSM temperature profile.

To compare the FEA results with the PSM measurements, we calculated the convolution of $\Delta T(\rho)$ with a step function with amplitudes changing from $+1$ to -1 at the boundary position (representing the polarization profile determined from the PFM image). The edge profiles from the thermal model shown in Fig. 4(d) agree well with the experimental profiles shown in Fig. 3(e), where both exhibit a sharper edge at higher modulation frequency. To quantify the resolution, we calculated the width of the transition edge $w = (J^+ - J^-)/2J'$, where J^+ and J^- are the maximum and minimum amplitudes around the two edges and J' is the slope of the profile at the midpoint.[54] The dependence of the edge width $w(f)$ on modulation frequency from both the

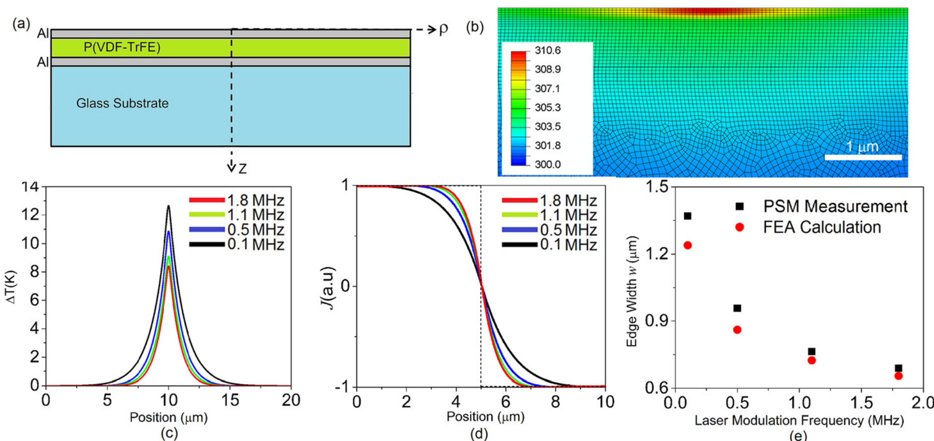

FIG. 4. Thermal model of the sample implemented FEA. (a) Sample cross-section. (b) The average temperature profile after 5 μs. (c) The z-averaged lateral distribution of the temperature modulation amplitude $\Delta T(\rho)$ in the polymer film layer for four different modulation frequencies. (d) The convolution of $\Delta T(\rho)$ at four frequencies with the reference step function (in dashed line). (e) The experimental values of the PSM imaging resolution compared with the values calculated from the curves in (d).

experiment (Fig. 3(e)) and the model (Fig. 4(d)) are shown in Fig. 4(e). The two results agree very well, without using any adjustable parameters in the model. At the highest frequency, 1.8 MHz, the PSM data have an edge width of 660 ± 28 nm, vs. 630 ± 10 nm from the model. These values are both larger than the measured beam size of 352 ± 14 nm, which is likely due to a combination of factors, notably that the maximum modulation frequency, 1.8 MHz, is not high enough to make the diffusion length much smaller than the laser beam width. An additional contribution to blurring could come from drifting of the distance between the microscope objective and sample surface, which would enlarge the beam spot on the sample.

We have implemented a PSM system that achieves high resolution by means of a tightly focused violet laser beam for localized heating and high modulation frequency to minimize thermal diffusion. We have used the system to achieve a lateral resolution of 660 ± 28 nm when imaging the polarization pattern in a thin film of vinylidene fluoride copolymer. The results are in excellent agreement with a thermal model implemented by finite element analysis. The PSM system with submicron resolution is an efficient, non-invasive tool complementary to PFM in studies of thin film ferroelectric materials, and is uniquely valuable for studying nonferroelectric pyroelectric materials, which usually have negligible piezoresponse. PSM should be useful for testing pyroelectric devices, and in the development and characterization of ferroelectric and pyroelectric materials. The use of high modulation frequencies also permits studying transient polarization phenomena. There is, however, still room for improvement of PSM resolution. For example, near field optical microscopy (NSOM) can be used to overcome the optical diffraction limit and produce localized heating with a resolution of 100 nm or smaller.

We thank K. Cole for fruitful discussions, M. Negahban and R. Feng for assistance with the FEA modeling software. This work was supported by the U.S. Department of Energy, Office of Basic Energy Sciences, under Award No. DE-SC0004530.

[1]T. D. Binnie, H. J. Weller, Z. He, and D. Setiadi, IEEE Trans. Ultrason., Ferroelectr., Freq. Control **47**, 1413 (2000).
[2]A. J. Holden, IEEE Trans. Ultrason., Ferroelectr., Freq. Control **58**, 1981 (2011).
[3]Z. L. Wang, G. Zhu, Y. Yang, S. H. Wang, and C. F. Pan, Mater. Today **15**, 532 (2012).
[4]Y. Fujisaki, Jpn. J. Appl. Phys., Part 1 **52**, 040001 (2013).
[5]M. Zirkl, A. Haase, A. Fian, H. Schon, C. Sommer, G. Jakopic, G. Leising, B. Stadlober, I. Graz, N. Gaar, R. Schwodiauer, S. Bauer-Gogonea, and S. Bauer, Adv. Mater. **19**, 2241 (2007).
[6]J. Y. Li, L. Zhang, and S. Ducharme, Appl. Phys. Lett. **90**, 132901 (2007).
[7]Y. Yuan, Z. Xiao, B. Yang, and J. Huang, J. Mater. Chem. A **2**, 6027 (2014).
[8]F. Y. Lee, A. Navid, and L. Pilon, Appl. Therm. Eng. **37**, 30 (2012).
[9]X. Y. Li, S. G. Lu, X. Z. Chen, H. M. Gu, X. S. Qiana, and Q. M. Zhang, J. Mater. Chem. C **1**, 23 (2013).
[10]D. A. Bonnell, S. V. Kalinin, A. L. Kholkin, and A. Gruverman, MRS Bull. **34**, 648 (2009).
[11]A. Gruverman, O. Auciello, J. Hatano, and H. Tokumoto, Ferroelectrics **184**, 11 (1996).
[12]A. V. Bune, C. Zhu, S. Ducharme, L. M. Blinov, V. M. Fridkin, S. P. Palto, N. G. Petukhova, and S. G. Yudin, J. Appl. Phys. **85**, 7869 (1999).
[13]A. Hadni and R. Thomas, Ferroelectrics **4**, 39 (1972).
[14]A. Hadni, J. M. Bassia, X. Gerbaux, and R. Thomas, Appl. Opt. **15**, 2150 (1976).
[15]D. Royer, E. Dieulesaint, and P. Kummer, Electron. Lett. **20**, 583 (1984).
[16]F. Marlow, M. Wubbenhorst, and J. Caro, J. Phys. Chem. **98**, 12315 (1994).
[17]A. Quintel, J. Hulliger, and M. Wubbenhorst, J. Phys. Chem. B **102**, 4277 (1998).
[18]N. R. Behrnd, G. Couderc, M. Wubbenhorst, and J. Hulliger, Phys. Chem. Chem. Phys. **8**, 4132 (2006).
[19]T. Putzeys and M. Wubbenhorst, IEEE Trans. Dielectr. Electr. Insul. **19**, 1186 (2012).
[20]A. B. Bhattacharyya, S. Tuli, and S. Kataria, IEEE Trans. Instrum. Meas. **43**, 30 (1994).
[21]J. Groten, M. Zirkl, G. Jakopic, A. Leitner, and B. Stadlober, Phys. Rev. B **82**, 054112 (2010).
[22]A. Hadni, Ferroelectrics **140**, 25 (1993).
[23]A. Batagiannis, M. Wubbenhorst, and J. Hulliger, Curr. Opin. Solid State Mater. Sci. **14**, 107 (2010).
[24]M. Burgener, G. Labat, M. Bonin, A. Morelli, and J. Hulliger, CrystEngComm **15**, 7652 (2013).
[25]A. Hadni and R. Thomas, Ferroelectrics **7**(1–4), 177 (1974).
[26]M. Wegener, J. Hesse, T. Wegener, and R. Gerhard-Multhaupt, J. Appl. Phys. **91**, 3193 (2002).
[27]C. M. Othon and S. Ducharme, Appl. Phys. A **104**, 727 (2011).
[28]M. Stewart and M. Cain, J. Am. Ceram. Soc. **91**, 2176 (2008).
[29]G. J. Klap, S. M. van Klooster, M. Wubbenhorst, J. C. Jansen, H. van Bekkum, and J. van Turnhout, J. Phys. Chem. B **102**, 9518 (1998).
[30]S. Ducharme, S. P. Palto, and V. M. Fridkin, *in Ferroelectric and Dielectric Thin Films*, edited by H. S. Nalwa (Academic Press, San Diego, 2002), Vol. 3, pp. 545.
[31]B. W. Peterson, S. Ducharme, V. M. Fridkin, and T. J. Reece, Ferroelectrics **304**, 51 (2004).
[32]A. V. Sorokin, S. Ducharme, and V. M. Fridkin, J. Appl. Phys. **98**, 044107 (2005).
[33]A. Mellinger, R. Singh, M. Wegener, W. Wirges, R. Gerhard-Multhaupt, and S. B. Lang, Appl. Phys. Lett. **86**, 082903 (2005).
[34]S. B. Lang and D. K. Dasgupta, J. Appl. Phys. **59**, 2151 (1986).
[35]S. B. Lang, IEEE Trans. Dielectr. Electr. Insul. **11**, 3 (2004).
[36]D. Marty-Dessus, L. Berquez, A. Petre, and J. L. Franceschi, J. Phys. D: Appl. Phys. **35**, 3249 (2002).
[37]B. Ploss, R. Emmerich, and S. Bauer, J. Appl. Phys. **72**, 5363 (1992).
[38]S. B. Lang, IEEE Trans. Dielectr. Electr. Insul. **5**, 70 (1998).
[39]C. D. Pham, A. Petre, L. Berquez, R. Flores-Suarez, A. Mellinger, W. Wirges, and R. Gerhard, IEEE Trans. Dielectr. Electr. Insul. **16**, 676 (2009).
[40]S. V. Kalinin, A. Rar, and S. Jesse, IEEE Trans. Ultrason., Ferroelectr., Freq., Control **53**, 2226 (2006).
[41]B. J. Rodriguez, A. Gruverman, A. I. Kingon, R. J. Nemanich, and J. S. Cross, J. Appl. Phys. **95**, 1958 (2004).
[42]M. Alexe and A. Gruverman, *in Nanoscience and Technology* (Springer-Verlag, Berlin, New York, 2004), p. 282.
[43]A. Quintel, S. W. Roth, J. Hulliger, and M. Wubbenhorst, Mol. Cryst. Liq. Cryst. **338**, 243 (2000).
[44]M. J. Bai, A. V. Sorokin, D. W. Thompson, M. Poulsen, S. Ducharme, C. M. Herzinger, S. Palto, V. M. Fridkin, S. G. Yudin, V. E. Savchenko, and L. K. Gribova, J. Appl. Phys. **95**, 3372 (2004).
[45]A. V. Bune, V. M. Fridkin, S. Ducharme, L. M. Blinov, S. P. Palto, A. V. Sorokin, S. G. Yudin, and A. Zlatkin, Nature (London) **391**, 874 (1998).
[46]J. Choi, C. N. Borca, P. A. Dowben, A. Bune, M. Poulsen, S. Pebley, S. Adenwalla, S. Ducharme, L. Robertson, V. M. Fridkin, S. P. Palto, N. N. Petukhova, and S. G. Yudin, Phys. Rev. B **61**, 5760 (2000).
[47]B. E. A. Saleh and M. C. Teich, *Fundamentals of Photonics* (Wiley, New York, 1991).
[48]B. J. Rodriguez, S. Jesse, S. V. Kalinin, J. Kim, S. Ducharme, and V. M. Fridkin, Appl. Phys. Lett. **90**, 122904 (2007).
[49]P. Sharma, T. Reece, D. Wu, V. M. Fridkin, S. Ducharme, and A. Gruverman, J. Phys. Condens. Matter **21**, 485902 (2009).
[50]P. Sharma, D. Wu, S. Poddar, T. J. Reece, S. Ducharme, and A. Gruverman, J. Appl. Phys. **110**, 052010 (2011).
[51]P. Sharma, T. J. Reece, S. Ducharme, and A. Gruverman, Nano Lett. **11**, 1970 (2011).
[52]R. N. Bracewell, *The Fourier Transform and its Applications*, 2nd ed. (McGraw-Hill, New York, 1978).
[53]N. Stojanovic, J. S. Yun, E. B. K. Washington, J. M. Berg, M. W. Holtz, and H. Temkin, J. Microelectromech. Syst. **16**, 1269 (2007).
[54]S. V. Kalinin, S. Jesse, B. J. Rodriguez, J. Shin, A. P. Baddorf, H. N. Lee, A. Borisevich, and S. J. Pennycook, Nanotechnology **17**, 3400 (2006).